https://doi.org/10.48048/tis.2022.1329

Study of Low-Frequency Electromagnetic Ion-Cyclotron Wave for Ring Distribution in Magnetosphere of Saturn

Annex Edappattu Haridas and Rama Shankar Pandey*

Department of Physics, Amity Institute of Applied Sciences, Amity University, Uttar Pradesh, India

(*Corresponding author's e-mail: rspandey@amity.edu)

Received: 16 December 2021, Revised: 12 April 2022, Accepted: 19 April 2022, Published: 5 November 2022

Abstract

Magnetic cyclotron waves were discovered by the Cassini-Huygens spacecraft in Saturn's atmospheric torus' magnetic layer. They are left-handed and propagate at a minor angle to the ambient magnetic field in most areas because their frequency is close to the frequency of the aqua ions. The ion cyclotron instability caused by Saturn's neutral cloud ions helps explain their formation. They can be classified as n = 2 mode fluctuations because of the ion-ring distribution. We planned the characteristics of these waves in advance of starting this project. Our dispersion growth rates are evaluated using kinetic method analysis as well. The results were calculated and explained for the exemplary values of the magnetosphere parameters suitable for Saturn. Another potential free energy source for ion cyclotrons is temperature anisotropy. Instead of the standard Maxwell distribution, a ring distribution is employed in this study. The focus of this research is EMIC waves' oblique propagation in the magnetic field, which changes their temperature anisotropy, ion energy density, and propagation angle. The interaction of relativistic particles with ion cyclotron waves is also included in this extension. EMIC wave size decreases with the increasing density of particles, as shown by a numerical study. A comparison of planetary studies based on data from space plasma environments and magnetospheric systems produced these results.

Keywords: Ion cyclotron waves, Relativistic particles, Ring distribution, Saturn magnetosphere

Introduction

Electromagnetic cyclotron waves are generally believed responsible for angular pitch spreading and thin-layer ion precipitation loss in the planetary atmosphere. This specific example concerns earth's circulation [1,2], Jupiter's magnetosphere [3-5], and the anisotropic thermionic ions' magnetosphere [6]. High-frequency EMIC wave analysis in the magnetospheric region induces perpendicular heating [7]

Electro Magnetic Ion-Cyclotron (EMIC) is suspended in a plasma layer over the plasma edge with frequencies between 1.0 and 5,0 Hz or in the drainage column. All of these waves have the ability to produce 3 different elements: Hydrogen (H+), helium (He+), and oxygen (O+). The EMIC dispersion curve is shown in Section 3 [8,9]. (L-mode). EMIC waves increase in electro-magnetic storms (13; 5; 10). The EMIC wave offers a free source of energy in the form of a low-energy circulating hydrogen (H +) anisotropic distribution [10]. Study highlights the role of energetic electrons on the wave spectrum, using Vlasov-Maxwell's model [11].

The nature of the ion, geomagnetic activity, and geographical position all influence the band of the awakened EMIC wave [12]. Despite the fact that the storm time relativistic drift orbit (> 1 MV) briefly crosses the EMIC wave's excitation zone, EMIC wave magnitudes, corner dispersion, and precipitation loss are often bigger than the EMIC local region.

Theoretically, Summers and Thorne [13] investigated how the EMIC Wave/Electron Resonance Interaction's lowest energy relies on the EMIC spectrum and composite ion properties. [14] EMIC has an average spectral intensity of 4-5nT/Hz which is sufficient to extend the pitch angle of the electron to its upper limit.

Materials and methods

The frequency of an ionic cyclotron wave is determined by the initial ion and the local strength of the magnetic field. The magnetic properties of the Comet [15] and Jupiter's layers [6,16]. These waves demand a lot more free energy than the temperature parallel to the magnetic field [17]. Precipitation of energetic protons further impacts the ionosphere-thermosphere and contribute to the ionization in the E/F regions [18]. The most unstable distribution is a cold neutral ionisation in a ring magnet flow. In the speed range,

these ions create a tiny ring around the magnetic field's direction. Pioneer 11 discovered ion cyclotron waves for the first time in Saturn's E orbit (6.26 R_s) [6]. Magnet vibrations from 5 to 7 radial lengths were discovered by Voyager 1 [19]. The anisotropic temperature of the O+ population is thought to be connected to these wave measurements. Cassini studied the shifting seasons, viewed Saturn's unusual storms and jet streams up close, and heard Saturn's lightning, which cannot be detected from Earth. It plunged into the gap between Saturn and its rings during the Grand Finale orbits, gathering crucial data on Saturn's internal structure and spin [20,21].

Once again, the water group ion cyclotron pulse on the Cassini path was recognised by the magnetometer [22,23]. Studied the structure and dynamics and the solar cycle and seasonal modulations of the plasma located between 2.5 and 12 Saturn radii (1 R_S = 60, 268 km) from Saturn [24]. Analytical equations incorporate all of the relevant magnetic field-aligned forces acting on the plasma and allow us to determine the spatial distribution of the 2 major ion components in terms of equatorial ion densities and scale heights [25]. In the current work, we have studied the interaction in Saturn's magnetosphere using electromagnetic ion cyclotron waves between relativistic and non-relativistic particles. The disturbed distribution function, particle path and growth rate are expressed in a lengthy mathematical formulation for oblique propagation utilising dynamics and characteristic approaches. Various plasma variables were studied to determine their impact on growth rates.

Mathematical formulation

An anisotropy of a magnetic field with an amplitude in the direction of Z is postulated and plasma is free of collisions and uniform. In the current example, the region of interaction is considered to be less uneven. For the disruptive distribution function and dispersion relationship-specific trajectory, Vlasov Maxwell is used. After dividing the equalising component and the non-equilibrium element, the linearized Vlasov equations were ignored and following the technique and method of Kumari and Pandey [26] and Shukla *et al*. [27]:

$$\left(\frac{\partial f_o}{\partial r}\right) + \left(\frac{e}{m_s}\right)\left[\frac{(v \times B_o)}{c}\right] \cdot \left(\frac{\partial f_o}{\partial v}\right) = 0 \quad (1)$$

$$\left(\frac{\partial f_1}{\partial t}\right) + v \cdot \left(\frac{\partial f_1}{\partial r}\right) + \left(\frac{F}{m_s}\right) \cdot \left(\frac{\partial f_1}{\partial v}\right) = S(r, v, t) \quad (2)$$

where the force

$$F = e\frac{(v \times B_o)}{c} = m_s \frac{dv}{dt} \quad (3)$$

Now, we have written all the equations in terms of momentum instead of velocity for relativistic particles and introduce relativistic factor which is defined as $\beta = \frac{1}{\sqrt{1-\frac{v^2}{c^2}}}$.

The dispersion relationship is described as follows:

$$S(r_o, p_o, t - t') = -\left(\frac{-e_s}{m_s \omega}\right) \exp\left[i\left(k \cdot r_o(r, p, t') - \omega(t - t')\right)\right] * [(\omega - k \cdot v_o)E_1 + (v_o \cdot E_1)k] \cdot \left(\frac{\delta f_s}{\delta p}\right) \quad (4)$$

The electron type is denoted by the letter s. The balance values are denoted by the 'o' subscript. Using the feature technique, the disturbed distribution function f_{s1} is calculated.

$$f_{s1}(r, p, t) = \int_0^\infty S\{r_0(r, p, t'), p_o\ (r, p, t'), (t - t')\}dt'$$

$(r_o, p_o, t - t')$ has been replaced as the phase coordinate system for (r, p, t). The particle routes determined from solving Eq. (3) for given external field configuration are as follows:

$$X_o = X + \left(\frac{p_\perp \sin\theta}{\omega_c m_s}\right) - \left[\frac{p_\perp}{\omega_c m_s} \sin\left\{\theta + \frac{\omega_c t}{\beta}\right\}\right]$$

$$Y_o = Y - \left(\frac{p_\perp \cos\theta}{\omega_c m_s}\right) + \left[\frac{p_\perp}{\omega_c m_s} \cos\left\{\theta + \frac{\omega_c t}{\beta}\right\}\right]$$

$$Z_o = Z - \frac{p_{||}}{\beta m_s} t \tag{5}$$

and the velocities are:

$$v_{xo} = \frac{p_\perp}{\beta m_s} \cos\left\{\theta + \frac{\omega_c t}{\beta}\right\}$$

$$v_{yo} = \frac{p_\perp}{\beta m_s} \sin\left\{\theta + \frac{\omega_c t}{\beta}\right\}$$

$$v_{zo} = \frac{p_{||}}{\beta m_s} \tag{6}$$

where $m_e = \frac{m_s}{\beta}$ and $\omega_c = \frac{eB_o}{m_s}$ = Electron cyclotron frequency.

Perpendicular magnetic field moments are denoted by the symbols $p_\perp$ and $p_{||}$. To obtain the perturbed distribution function, we first simplify the algebra using equations (27), and the Bessel identity. Next we complete the time integration.

$$f_1 = -\left(\frac{ie}{\beta m_s \omega}\right) \sum_{m,n,p=-\infty}^{\infty} \exp i(m-n)\theta \left[\frac{J_m(\lambda_1)}{\omega - \frac{k_{||} p_{||}}{\beta m_s} - \frac{n\omega_c}{\beta}}\right] \left[U^* E_{1x} \frac{n}{\lambda_1} J_n(\lambda_1) + iU^* E_{1y} J_n'(\lambda_1) + W^* E_{1z} J_n(\lambda_1)\right] \tag{7}$$

when m = n, the solution is achievable because to the phase factor. Here:

$$U^* = C + F$$

$$W^* = B\left(\frac{n m_s \omega_c}{k_\perp p_\perp}\right) + (\beta m_s \omega) \frac{\partial f_o}{\partial p_\perp}$$

$$B = (\beta m_e) \frac{\partial f_o}{\partial p_{||}} \left(\frac{k_\perp p_\perp}{\beta m_e}\right)$$

$$C = \frac{(\beta m_e)^2}{p_\perp} \frac{\partial f_o}{\partial p_\perp} \left(\omega - \frac{k_{||} p_{||}}{\beta m_e}\right) \frac{p_\perp}{\beta m_e}$$

$$F = (\beta m_e) \frac{\partial f_o}{\partial p_{||}} \left(\frac{k_{||} p_\perp}{\beta m_e}\right)$$

(8)

$$J_n'(\lambda_1) = \frac{dJ_n(\lambda_1)}{d\lambda_1}$$

The Bessel function argument is defined as:

$$\lambda_1 = \frac{k_\perp p_\perp}{\omega_c m_s}$$

The conductivity tensor $\| \sigma \|$ is found to be:

$$\| \sigma(k, \omega) \| = -i \sum_s \frac{e_s^2}{(\beta m_s} \sum_n \left[\frac{S_{ij}^*}{\omega - \frac{k_{||} p_{||}}{\beta m_s} - \frac{n\omega_c}{\beta}}\right]$$

where

$$\left\|S_{ij}^{*}\right\| = \begin{vmatrix} p_{\perp}U^{*}\left(\frac{n}{\lambda_1}\right)^{2}J_n^2 & ip_{\perp}U^{*}\left(\frac{n}{\lambda_1}\right)J_nJ_n^{'} & p_{\perp}W^{*}\left(\frac{n}{\lambda_1}\right)J_n^2 \\ ip_{\perp}U^{*}\left(\frac{n}{\lambda_1}\right)J_nJ_n^{'} & -p_{\perp}U^{*}(J_n^{'})^2 & ip_{\perp}W^{*}J_nJ_n^{'} \\ p_{||}U^{*}\left(\frac{n}{\lambda_1}\right)J_n^2 & ip_{||}U^{*}J_nJ_n^{'} & p_{||}W^{*}J_n^2 \end{vmatrix}$$

We get the dielectric tensor by plugging these into Maxwell's equations.

$$\varepsilon_{ij}(k,\omega) = 1 + \sum_s \frac{4e_s^2\pi}{(\beta m_s)^2\omega^2}\sum_n \int \frac{\left\|S_{ij}^{*}\right\|d^3p}{\omega - \frac{k_{||}p_{||}}{\beta m_s} - \frac{n\omega_c}{\beta}} \tag{9}$$

The generic dispersion relation simplifies to electromagnetic ion cyclotron instability;

$\varepsilon_{11} + i\varepsilon_{12} = N^2$where $N^2 = \frac{k^2c^2}{\omega^2}$.

The particle trajectory, the disturbance function, the conductivity tensor and the dispersion of the relativistic condition must be described in the absence of an electric field as:

$$\frac{k^2c^2}{\omega^2} = 1 + \sum_s \frac{4e_s^2\pi}{(\beta m_s)^2\omega^2}\sum_p J_p(\lambda_2)\int \frac{d^3p}{2} p_{\perp}\left[(\beta m_s)\left(\omega - \frac{k_{||}p_{||}}{\beta m_s}\right)\frac{\partial f_o}{\partial p_{\perp}} + k_{||}p_{\perp}\frac{\partial f_o}{\partial p_{||}}\right] * \left(\frac{1}{\omega - \frac{k_{||}p_{||}}{\beta m_s} \pm \frac{\omega_c}{\beta}}\right) \tag{10}$$

[26,27] have all detailed the Maxwellian ring distribution function for trapped electrons:

$$f\left(v_{\perp}, v_{||}\right) = \frac{\frac{n_s}{n}}{\pi^{3/2}p_{o||s}p_{o\perp s}^2}\exp\left[-\frac{(p_{\perp}-p_o)^2}{p_{o\perp s}^2} - \frac{p_{||}^2}{p_{o||s}^2}\right] \tag{11}$$

$$A = \exp\left(-\frac{p_o^2}{p_{o\perp s}^2}\right) + \sqrt{\pi}\left(\frac{p_o}{p_{o\perp s}}\right)\operatorname{erfc}\left(-\frac{p_o}{p_{o||s}}\right) \tag{12}$$

where s stands for species of electrons and ions are taken into consideration in this example,

$p_{o\|e} = \left(\frac{k_B T_{\|e}}{\beta m_e}\right)^{1/2}$, $p_{o\perp e} = \left(\frac{k_B T_{\|\perp e}}{\beta m_e}\right)^{1/2}$, $p_{o\|i} = \left(\frac{k_B T_{\|e}}{\beta m_i}\right)^{1/2}$, and $p_{o\perp i} = \left(\frac{k_B T_{\perp i}}{\beta m_i}\right)^{1/2}$

are the ions' and electrons' thermal velocities in parallel and perpendicular directions.

Another error function is the electron-to-total-electron-density ratio, which is represented by high energy in Eq. (11) ns/n. With regard to the magnetic field, the thermal velocities in perpendicular and parallel directions are denoted as $p_{\perp}$ and $p_{\|}$.The drift velocity in terms of momentum is represented as p_o.

Governing dispersion relation

Substituting $d^3p = 2\pi\int_0^{\infty} p_{\perp}dp_{\perp}\, d\int_{-\infty}^{\infty} dp_{||}$and we derive the dispersion relation as: utilising the expression Eq. (11) in Eq. (10) and after resolution of the integrations:

$$\frac{k^2c^2}{\omega^2} = 1 + \frac{4e_s^2\pi}{(\beta m_s)^2\omega^2}\sum_p J_p(\lambda_2)\frac{(n_s/n)}{A}(\beta m_s)\left[\frac{\beta m_s}{p_{o||s}}\left(\frac{\omega}{k_{||}}\right)X_1 Z(\xi) + X_2\left(1 + \xi Z(\xi)\right)\right] \tag{13}$$

The above dispersion relation is now approximated in ion cyclotron range of frequencies. In this case electron temperature are assumed as $T_{\perp e} = T_{\|e} = T_e$ and magnetized with$\left|\omega_r + i_{\gamma}\right| \ll \omega_{ci}$ whereas ions are assumed to have $T_{\perp i} > T_{\|i}$ and $|k_{\perp i} \propto_{\|i} \ll |\omega_r \pm \omega_{ci} + i\gamma|$. So considering the above approximations, Eq. (13) is reduced to:

$$D(k,\omega_r + i\gamma) = 1 - \frac{k^2c^2}{(\omega_r+i\gamma)^2} + \sum_p J_p(\lambda_2)\left[\left(\frac{\omega_{pe}^2}{\omega_{ci}^2} - \frac{\omega_{pe}^2}{(\omega_r+i\gamma)(\pm\omega_{ci})}\right)X_{ie}(\beta m_e) + \frac{\omega_{pi}^2}{(\omega_r+i\gamma)^2}\left(X_{1i}\frac{(\beta m_i)}{p_{o||i}}\left(\frac{\omega_r+i\gamma}{k_{||}}\right)Z(\xi_i) + X_{2i}\left(1 + \xi_i Z(\xi_i)\right)\right)\right] \tag{14}$$

where,

$$X_{1i} = 1 + \frac{p_o^2}{p_{o\perp i}^2} - \sqrt{\pi}\frac{p_o}{p_{o\perp i}}$$

$$X_{1e} = 1 + \frac{p_o^2}{p_{o\perp e}^2} - \sqrt{\pi}\frac{p_o}{p_{o\perp e}}$$

and

$$X_{2i} = X_{1i} + \frac{p_{\perp i}^2}{p_{o||i}^2}\left(1 - \sqrt{\pi}\frac{p_o^3}{p_{o\perp i}^3}\operatorname{erfc}\left(\frac{p'_{\perp i}}{p_{o\perp i}}\right) + 3\frac{p_o^2}{p_{o\perp i}^2} - \frac{3}{2}\sqrt{\pi}\frac{p_o}{p_{o\perp i}}\right)$$

After applying charge neutrality condition $\frac{\omega_{pe}^2}{\pm\omega_{ce}^2} = \frac{-\omega_{pi}^2}{\pm\omega_{ci}^2}$ and the condition $\left|\frac{k^2c^2}{\omega^2} \gg 1 + \frac{\omega_{pe}^2}{\omega_{ce}^2}\right|$, the dispersion relation reduces to:

$$D(k, \omega_r + i\gamma) = -\frac{k_{||}^2c^2}{\omega_{pi}^2} + \sum_p J_p(\lambda_2)\left[\frac{\omega}{\pm\omega_{ci}}(\beta m_e)X_{1e} + (\beta m_i)X_{1i}\left\{\frac{\beta m_i}{p_{o||i}}\left(\frac{\omega}{k_{||}}\right)Z(\xi_i) + \frac{X_{2i}}{X_{1i}}\left(1 + \xi_i Z(\xi_i)\right)\right\}\right] \quad (15)$$

The purpose of plasma dispersion is as follows $Z(\xi) = \frac{1}{\sqrt{\pi}}\int_{-\infty}^{\infty}\frac{e^{-t^2}}{t-\xi}dt$, where

$$\xi = \frac{\beta m_i\omega \pm m_i\omega_c}{k_{||}p_{o||i}}$$

$$\omega_{pi}^2 = \frac{4\pi e^2}{(\beta m_i)^2}\frac{n_i/n}{B}$$

Now, dimensionless parameter $\tilde{k}$ called as wave vector is introduced.

Expression of growth rate

The real frequency and growth rate of the ion cyclotron spread to the magnetic field are as follows:

$$\frac{\gamma}{\omega_{ci}} = \frac{\frac{\sqrt{\pi}}{\tilde{k}\cos\theta}\left(\frac{X_{2i}}{X_{1i}} - k_4\right)k_3^3\exp\left[-\left(\frac{k_3^2}{\tilde{k}\cos\theta}\right)^2\right]}{1 + \frac{(\tilde{k}\cos\theta)^2}{2k_3^2} + \frac{(\tilde{k}\cos\theta)^2}{k_3}\left(\frac{X_{2i}}{X_{1i}} - k_4\right) + \frac{m_eX_{1e}}{m_iX_{1i}}k_3^2} \quad (16)$$

The real part of Eq. (16) is:

$$X_3 = -\frac{\beta\omega_r}{\omega_c} = X_4 + \frac{\left(\tilde{k}\cos\theta\right)^2}{2\beta_1}\left[\frac{X_{2i}}{X_{1i}}\frac{\beta_1}{(1+X_4)} - \frac{(1+X_4)}{\beta X_{1i}}\right]$$

$k_{||} = k\cos\theta$ and $\tilde{k} = \frac{\beta k\, p_{o||}}{\omega_{ci}}$

Results and discussion

We examined the overall behaviour of an ion cyclotron instability due to the existence in this article of a ring distribution function in the magnetosphere of Saturn. According to the Voyager report, the ion count varies from 3×10^7 to 7×10^7 m^{-3}, which is more in accordance with 2013 Ahirwar's [28,29] magnetosphere observations at 3.9 R_s radial distance and 1keV thermal energy. The magnetic field had a power of 300 nT, while the ion gyros had a frequency of 28.7 Hz. For this experiment, electrons had an energy range of 15 - 300 eV.

As mentioned above, the growth rate with the wave number is determined according to the plasma parameters and field parameters L = 3.9 and expression of the growth rate given in the Eq. (16). The

estimated wave count growth rate indicates a major peak at normalised frequency < 1 and always accompanied by reduced wave count following growth (**Figures 1 - 7**). It can also be observed that the existence of a relativistic electron tail leads to a major shift in the normalised rate of increase at the lower peak. **Figure 1** shows that an increase in ion number density will decrease EMIC instability's peak growth rate. **Figure 2** indicates that a minor decrease in the maximum value of the ion cyclotron wave comes from the rise in the relative factor while, as shown in **Figure 3**, the increase in temperature anisotropy considerably increases the peak value. The increase in the cyclotron ion propagation angle does not alter its peak but changes the wave number to higher spectra and the pace of growth is barely affected by changes in temperature anisotropy at lower wave frequencies. The result is seen in **Figure 4**. In **Figures 5 - 7**, the influence of numerical density and temperature anisotropy on non-relativist electrodes is demonstrated. When the non-relativist impact was taken into account, the rise in the number density, compared with the relativistic effect, increased the peak and moved it to the bottom side of the wave. If 2 examples are studied individually, the anisotropic temperature impact is not evident. As a result, the presence of relativistic electrons has no effect on the rate of growth generated by temperature anisotropy. Figure 8 shows the relationship between the actual frequency and the rate of wave expansion. As can be seen from the real frequency and growth rates, the mathematical model's true frequency for ion cyclotron stability is far higher than the expected growth rate. These results are consistent with prior research. Others have used a ring distribution function to demonstrate relativistic effects and the impact of various instabilities on extremely low frequency radiation in this work. The growth rate corresponds to the literature provided by Ahmad and Ahmad [30]. They computed ion cyclotron growth rate propagating with parallel AC electric field in Jupiter magnetospheres.

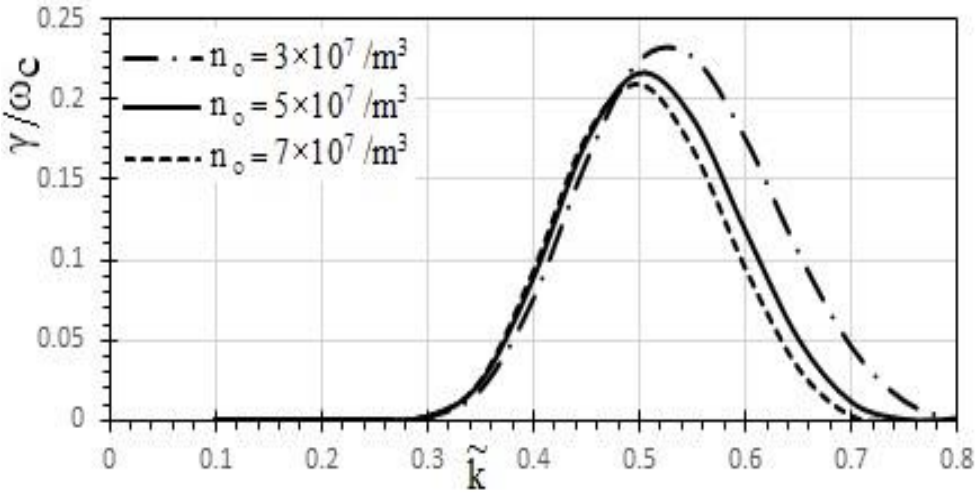

Figure 1 Variation of growth rate for relativistic particle with $\tilde{k}$ relative to different values of number density n_0 at B_o = 300 nT, K_BT_{lli} = 1 keV, K_BT_{lle} = 200 eV, A_T = 1.5, $\theta = 10^O$and β = 0.5 at 3.9 R_S.

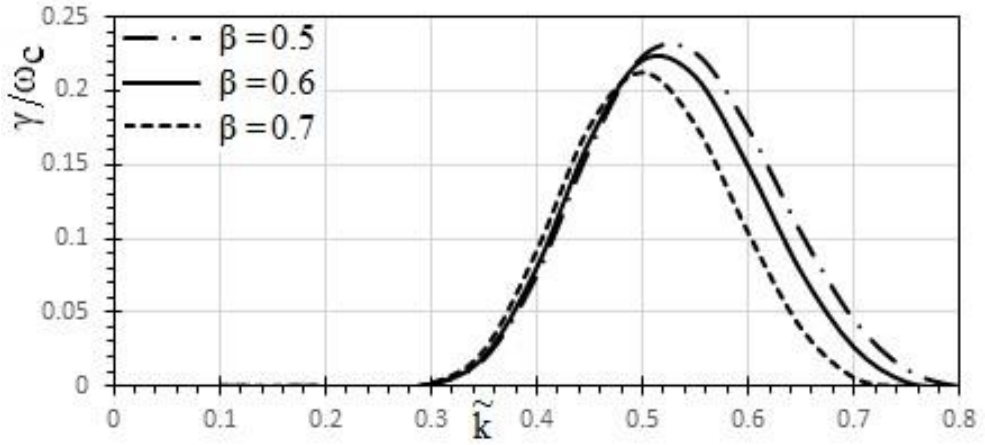

Figure 2 Variation of growth rate for relativistic particle with $\tilde{k}$ relative to different values of relativistic factor at $n_0 = 5\times10^7\ m^{-3}$, $B_o = 300nT$, $K_BT_{lli} = 1$ keV, $K_BT_{lle} = 200eV$, $A_T = 1.5$ and $\theta = 10^O$ at 3.9 R_S.

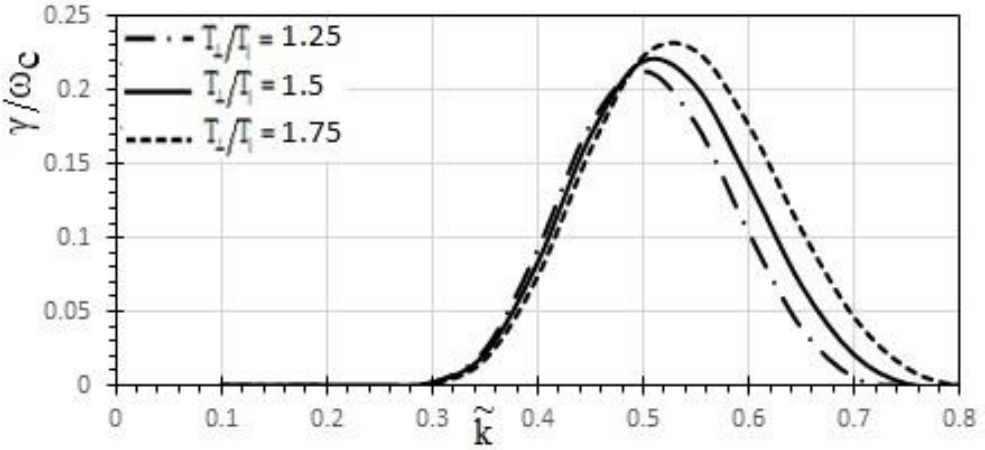

Figure 3 Variation of growth rate for relativistic particle with $\tilde{k}$ relative to different values of temperature anisotropy at $n_0 = 5\times10^7\ m^{-3}$, B_o=300nT, $K_BT_{lli} = 1$ keV, $K_BT_{lle} = 200eV$,$\theta = 10^O$, $A_T = 1.5$ and $\beta = 0.5$ at 3.9 R_S.

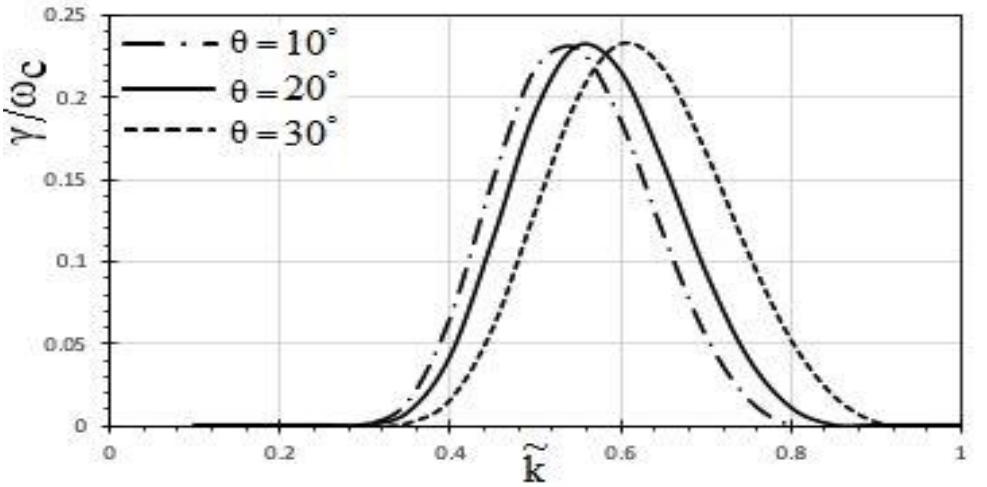

Figure 4 Variation of growth rate for relativistic particle with $\tilde{k}$ relative to different values of angle of propagation at $n_0 = 5\times10^7\ m^{-3}$, B_o= 300 nT, $K_BT_{lli} = 1$ keV, $K_BT_{lle} = 200$ eV, $A_T = 1.5$ and $\beta = 0.5$ at 3.9 R_S.

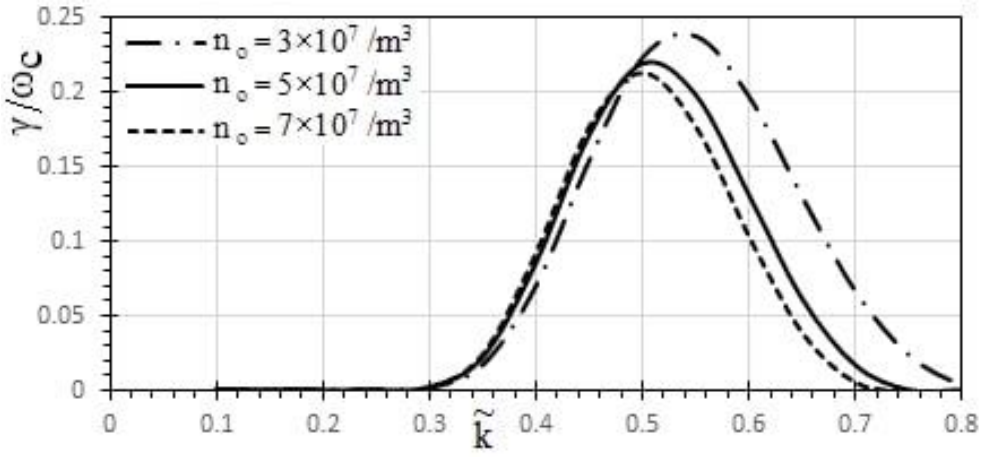

Figure 5 Variation of growth rate for non-relativistic particle with $\tilde{k}$ relative to different values of number density n_0 at B_o = 300 nT, K_BT_{lli} = 1 keV, K_BT_{lle} = 200eV, A_T = 1.5 and $\theta = 10^O$at 3.9 R_S.

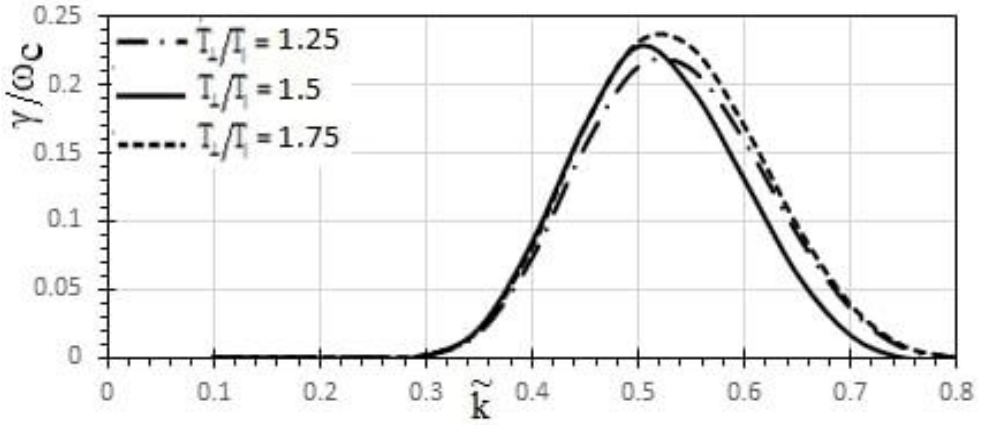

Figure 6 Variation of growth rate for non-relativistic particle with $\tilde{k}$ relative to different values of temperature anisotropy at $n_0 = 5\times10^7$ m^{-3}, B_o = 300 nT, K_BT_{lli} = 1 keV, K_BT_{lle} = 200eV and $\theta = 10^O$at 3.9 R_S.

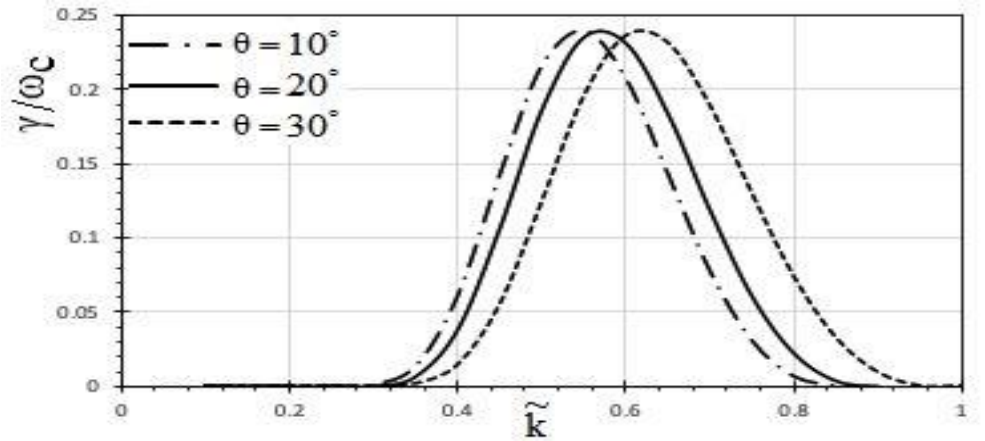

Figure 7 Variation of Growth Rate for Relativistic particle with $\tilde{k}$ relative to different values of angle of propagation at $n_0 = 5\times10^7$ m^{-3}, B_o = 300 nT, K_BT_{lli} = 1 keV, K_BT_{lle} = 200 eV and A_T = 1.5 at 3.9 R_S.

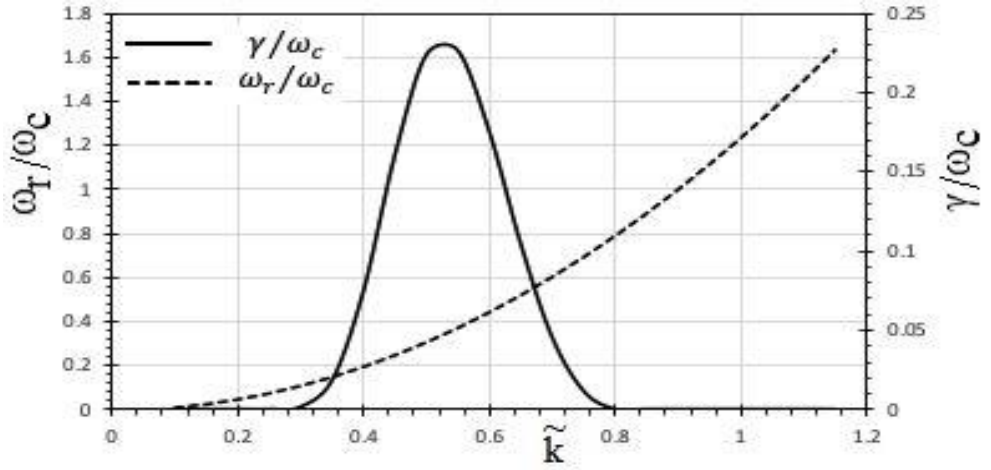

Figure 8 Variation of growth rate and real frequency with $\tilde{k}$ relative to different values of plasma parameters.

Conclusions

A magnetosphere wave propagates in Saturn's atmosphere in an oblique fashion when there isn't an electrical field distributing rings like there is on Earth. A kinetic method is utilised to test effectiveness, homogeneity and other characteristics at a radial radius of 3.9 R_s. For analysing the influence of plasma anisotropy, relativistic factors and spread angle and number density, dispersion relation, growth rate and real expressions of frequency are created. The results may show that if the value of the magnetosphere and the rate of growth of the relativistic and non-relativistic effects of the Saturn growth of the EIC wave were shifted to the lower wave, the value of the count of density would change.

Conversely, an increase in the spreading angle means that the wave that spreads oblique and the high-energy particle do not have a resonant interaction. Temperature anisotropy in the Saturnian magnetosphere with greater anisotropic temperature rates can likewise be seen as a significant source of free energy.

References

[1] JM Cornwall. Cyclotron instabilities and electromagnetic emission in the ultralow frequency and very low frequency ranges. *J. Geophys. Res*. 1965; **70**, 61.

[2] JM Cornwall, FV Coroniti and RM Thorne. Turbulent loss of ring current protons. *J. Geophys. Res.* 1970; **75**, 4699.

[3] FV Coroniti, CF Kennel and RM Thorne. Stably trapped proton fluxes in the Jovian magnetosphere. *Astrophys. J.* 1974; **189**, 383.

[4] A Eviatar, Y Mekler and FV Coroniti. Jovian sodium plasma. *Astrophys. J*. 1976; **205**, 622.

[5] RM Thorne. *Microscopic plasma processes in the Jovian magnetosphere*. *In*: AJ Dessler (Ed.). *Physics of the Jovian magnetosphere*. Cambridge University, New York, 1983, p. 454-88.

[6] EJ Smith and BT Tsurutani. (1983) Saturn's magnetosphere: Observations of ion cyclotron waves near the Dione L shell. *J. Geophys. Res.* 1983; **88**, 7831.

[7] K Min, J Kim, Q Ma, CW Jun and K Liu. Unusual high frequency EMIC waves: Detailed analysis of EMIC wave excitation and energy coupling between EMIC and magnetosonic waves. *Advances in Space Research.* 2021; **69**, 35-47.

[8] D Summers, B Ni and NP Meredith. Timescales for radiation belt electron acceleration and loss due to resonant wave-particle interactions: 2. Evaluation for VLF chorus, ELF hiss, and electromagnetic ion cyclotron waves. *J. Geophys. Res. Space Phys*. 2007; **112**, A04207.

[9] C Lacombe, O Alexandrova, L Matteini, O Santol´ık, N Cornilleau-Wehrlin, A Mangeney, YD Conchy and M Maksimovic. Whistler mode waves and the electron heat flux in the solar wind: Cluster observations. *Astrophys. J.* 2014; **796**, 5.

[10] VK Jordanova, CJ Farrugia, RM Thorne, GV Khazanov, GD Reeves and MF Thomsen. Modeling ring current proton precipitation by electromagnetic ion cyclotron waves during the May 14 - 16, 1997, storm. *J. Geophys. Res.* 2001; **106**, 7-22.

[11] M Sarfraz, G Abbas, H Farooq and I Zeba. Impact of non-thermal electrons on spatial damping: A kinetic model for the parallel propagating modes. *Zeitschrift für Naturforschung A* 2021; **76**, 661-9.

[12] BJ Fraser and TS Nguyen. Is the plasmapause a preferred source region of electromagnetic ion cyclotron waves in the magnetosphere? *J. Atmos. Sol. Terr. Phys.* 2001; **63**, 1225-47.
[13] D Summers and RM Thorne. Relativistic electron pitch-angle scattering by electromagnetic ion cyclotron waves during geomagnetic storms. *J. Geophys. Res.* 2003; **108**, 1143.
[14] NP Meredith, RM Thorne, RB Horne, D Summers, BJ Fraser and RR Anderson. (2003). Statistical analysis of relativistic electron energies for cyclotron resonance with EMIC waves observed on CRRES. *J. Geophys. Res*. 2003; **108**, 1250.
[15] LC Lee. *Theories of nonthermal radiations from planets, in plasma waves and instabilities at comets and in magnetospheres.* American Geophysical Union, Washington DC, 1989, p. 239-49.
[16] MG Kivelson and DJ Southwood. Mirror instability II: The mechanism of nonlinear saturation. *J. Geophys. Res.*1996; **101**, 17365.
[17] X Tian, Y Yu, M Zhu, L Ma, J Cao, PR Shreedevi, VK Jordanova and SC Solomon. Effects of EMIC wave-driven proton precipitation on the ionosphere. *J. Geophys. Res. Space Phys*. 2022; **127**, e2021JA030101.
[18] X Blanco-Cano. Wave generation in moon-satellite interactions. *Adv. Space Res.* 2004; **33**, 2078-91.
[19] Ingersoll AP. Cassini exploration of the planet Saturn: A comprehensive review. *Space Sci. Rev.* 2020; **216**, 122.
[20] DD Barbosa. Theory and observations of electromagnetic ion cyclotron waves in Saturn's inner magnetosphere. *J. Geophys. Res*. 1993; **98**, 9345-50.
[21] EH Annex, S Kanwar and RS Pandey. Electromagnetic electron-cyclotron wave for ring distribution with alternating current (AC) electric field in Saturn magnetosphere. *J. Astron. Space Sci.* 2022 **39**, 35-42.
[22] C Marty and CC Zong. Distribution of water group ion cyclotron waves in the Ssturn's magnetosphere. *Earth Planets Space* 2017; **69**, 122.
[23] JS Leisner, CT Russell, KK Khurana, MK Dougherty and N André. Warm flux tubes in the e-ring plasma torus: Initial cassini magnetometer observations. *Geophys. Res. Lett*. 2005; **32**, L14S08.
[24] MKG Holmberg, O Shebanits, JE Wahlund, MW Morooka, E Vigren, N André, P Garnier, AM Persoon, V Génot and LK Gilbert. Density structures, dynamics, and seasonal and solar cycle modulations of Saturn's inner plasma disk. *J. Geophys. Res. Space Phys*. 2017; **122**, 12258-73.
[25] AM Persoon, DA Gurnett, O Santolik, WS Kurth, JB Faden, JB Groene, GR Lewis, AJ Coates, RJ Wilson, RL Tokar, JE Wahlund, M Moncuquet. A diffusive equilibrium model for the plasma density in Saturn's magnetosphere. *J. Geophys. Res.* 2009; **114**, A04211.
[26] K Jyoti and RS Pandey. Whistler mode waves for ring distribution with A.C. electric field in inner magnetosphere of Saturn. *Astrophys. Space Sci.* 2018; **363**, 249.
[27] KN Shukla, D Singh and RS Pandey. Analytical study of electromagnetic ion cyclotron wave for ring distribution with AC electric field in Saturn magnetosphere *J. Phys. Conf. Ser.* 2021; **1817**, 012020.
[28] G Ahirwar. Electromagnetic ion-cyclotron waves in Saturn's magnetosphere. *Res. J. Recent Sci*. 2013; **34-38**, 2277-502.
[29] MF Thomsen, DB Reisenfeld, DM Delapp, RL Tokar, DT Young, FJ Crary, EC Sittler, MA McGra and JD Williams. Survey of ion plasma parameters in Saturn's magnetosphere. *J. Geophys. Res.* 2010; **115**, A10220.
[30] MM Ahmad and A Ahmad. Jovian magnetospheric ion cyclotron instability in the presence of parallel electric field. *Earth Moon Planets* 1993; **60**, 211-24.